SAMSON: A Generalized Second-order Arnoldi Method for Reducing Multiple Source Linear Network with Susceptance *

Yiyu Shi, Hao Yu and Lei He
Electrical Engineering Dept., University of California at Los Angeles
{yshi,hy255,lhe}@ee.ucla.edu

ABSTRACT

Power integrity analysis of in-package and on-chip power supply needs to consider a large number of ports and handle magnetic coupling that is better represented by susceptance. The existing moment matching methods are not able to accurately model both large number of ports and susceptance. In this paper, we propose a generalized Second-order Arnoldi method for reducing Multiple Source Linear Network (SAMSON) with susceptance. We employ a right-hand-side excitation current vector to replace the port incident matrix such that an MIMO (Multiple-input-multiple-output) system is transformed into an equivalent superposed SIMO (Single-input-multiple-output) system to avoid accuracy loss in block moment matching, and develop a generalized second-order Arnoldi method based orthonormalization to accurately handle susceptance and non-impulse current sources. Compared with existing EKS and IEKS approaches able to consider non-impulse sources but not susceptance, SAMSON is slightly faster and is more accurate in high frequency range and at dc. With same model order, SAMSON reduces time domain waveform error by 33X compared to EKS/IEKS and by 47X compared with the best block moment matching method applicable to susceptance.

Categories and Subject Descriptors

J.6 [**Computer Applications**]: COMPUTER-AIDED ENGINEERING—*Computer-aided design (CAD)*

General Terms

Algorithms

1. INTRODUCTION

Package and power grid simulation is an essential part in modern VLSI design. Typical package and power grid circuits usually have millions of nodes and large numbers of ports. In addition, simulators must be able to handle inductance, especially for the package. Particularly, susceptance is the preferred model for inductance because susceptance matrix is usually diagonally dominant and can be sparsified by a simple truncation method without disrupting the positive definiteness [1, 2, 3]. In contrast, the partial inductance model results in a large and dense matrix difficult to sparsify.

There are two kinds of approaches to simulate package and power grids. One is partition and locality based reduction and the other approach is model order reduction (MOR). The former includes [4, 5]. [4] partitions power grids and maps internal sources to external ports. It needs additional sparsification which is time-consuming and not accurate. [5] proposed the localized simulation and design methods based on the locality of current distribution in most power grids with C4-bumps. However, the accuracy is limited for low frequency [5].

This paper focuses on MOR. There are two types of MOR. The first type, non-RHS (right-hand-side) MOR, performs MOR directly on the transfer function and then obtains output responses by convolving the reduced transfer function with the inputs. Non-RHS methods include the first order ones like PRIMA [6], and the second order ones like ENOR [7], SMOR [8] and SAPOR (Second-Order Arnoldi Method for Passive Order Reduction of RCS Circuits)[9, 10] that are applicable to susceptance. However, those methods are not accurate when the port number is large. Precisely, if the circuit has p ports and is reduced to order q, then only the first $\lfloor q/p \rfloor$ block moments are matched. In addition, the runtime increases heavily with the number of ports. Therefore, non-RHS MOR methods are not efficient for P/G and package simulation with many ports.

The second type of MOR includes [11], EKS [12] and IEKS [13]. They perform MOR for linear circuits with RHS current sources and can be called RHS MOR. For a different input source a new reduced model needs to be recalculated. However, due to the much reduced reduction time, the overall runtime is still less than the non-RHS MOR methods where the convolution with the reduced transfer function is needed for a new input. Therefore, when dealing with package and power grid simulation, RHS-MOR is more powerful. [11] first proposed such kind of RHS MOR method. However, it is an explicit moment matching method and suffers from numerical instability. To improve it, EKS [12] employs incremental orthonormalization algorithm and implicitly matches the moments of output vector. It expresses the

*This paper is partially supported by NSF CAREER award CCR-0093273/0401682 and a UC MICRO grant sponsored by Analog Devices, Intel and Mindspeed. Address comments to lhe@ee.ucla.edu.

ISPD'06, April 9–12, 2006, San Jose, California, USA.

PWL source as a sum of delayed ramps in Laplace domain

$$u(s) = \frac{1}{s^2}\sum_{i=0}^{k} r_i exp(-\tau_i s) \quad (1)$$

The expression contains $1/s$ and $1/s^2$ terms which become obstacle for the traditional Krylov subspace methods. EKS overcomes it by shifting the moments towards right in the frequency spectrum of $u(s)$. This leads to the loss of accuracy, however. IEKS [13] avoids moment shifting by showing that the -1_{st} and -2_{nd} moments of *finite-time* PWL sources are zero.

One important limitation of both EKS and IEKS is that they are in essence first order methods and cannot deal with RCS circuits with susceptance elements. Directly applying EKS or IEKS to an RCS circuit will not guarantee passivity [8]. Moreover, IEKS and EKS have limited accuracy since they both use incremental orthonormalization procedure and accumulative errors occurs during the procedure. This is analyzed in details in Section 2. In addition, they are not accurate to handle arbitrary independent current sources like

$$\begin{aligned} u_1(t) = sin(\omega t) \qquad & L(u_1) = \frac{\omega}{s^2+\omega^2} \\ u_2(t) = e^{-\alpha t} cos\omega t \qquad & L(u_2) = \frac{s+\alpha}{(s+\alpha)^2+\omega^2} \end{aligned} \quad (2)$$

which have $1/s^i$ terms (i is a positive integer). EKS needs to use moment shifting that is error-prone, and IEKS can not handle $1/s^i$ terms. Finally, IEKS cannot perform well in DC analysis because it can not consider $s = 0$, corresponding to the infinite time. *DC* analysis is closely related to power dissipation, local voltage spikes and ebbs on the Vdd (or Gnd) supply lines, and it is very important in power grid design.

In this paper, we develop an accurate yet efficient generalized Second-order Arnoldi Method for Reducing Multiple Source Network, namely SAMSON. It is an RHS MOR method. We theoretically show (see Theorem 3) why SAMSON can achieve better accuracy than non-RHS MOR. Simply speaking, by introducing *excitation current vector*, we can transform an MIMO (Multiple-input-multiple-output) system into an equivalent superposed SIMO (Single-input-multiple-output) system. Then we can match q moments of the output instead of the $\lfloor q/p \rfloor$ block moments for the original MIMO system. In addition, we develop a generalized second-order Arnoldi method based *orthonormalization procedure* to consider all kinds of non-impulse inputs precisely.

In short summary, SAMSON has the following three advantages:

1. Compared with block-SAPOR and other non-RHS MOR methods, it can match more moments of the output. Hence it is more accurate.
2. Compared with EKS and IEKS, it can deal with all kinds of RHS sources accurately without performing moment shifting or incremental orthonormalization algorithm. Therefore, it is numerically more stable, more efficient and more accurate in the whole frequency range especially at DC.
3. Compared with EKS and IEKS, it can deal with RCS circuit with guaranteed passivity.

N	the number of circuit nodes
p	I/O port number
q	the reduced order
$L^{n\times m}$	$n \times m$ space in Laplace domain
$R^{n\times m}$	$n \times m$ space in Real domain

Table 1: Notations

All these advantages are verified by experiments.

The rest of this paper is organized as follows: In Section 2, we review and analyze in details why non-RHS MOR methods cannot be accurate enough when dealing with large number of ports while SAMSON can. We also show the numerical error existing in EKS and IEKS. Our new method, SAMSON, is presented and analyzed in Section 3. Several numerical experiments on package and power grid simulation are provided in Section 4. Concluding remarks are given in Section 5.

2. PRELIMINARY

2.1 Limitation of Non-RHS MOR

For simplicity, we use the notation defined in Table 1. Considering the nodal analysis equations (NA), an RCS linear circuit can be expressed in Laplace domain as:

$$\begin{aligned} (G + sC + \Gamma/s)V(s) &= BJ_e(s) \\ y_e(s) &= LV(s), \end{aligned} \quad (3)$$

where $\Gamma = E_s^T L^{-1} E_s$ is the nodal susceptance matrix, and E_s is the adjacent matrix indicating the direction of inductance current flow.

Non-RHS model order reduction methods, like PRIMA [6] and block SAPOR [10], all assume impulse inputs and perform reduction on the transfer function, i.e.

$$H(s) = L(G + sC + \Gamma/s)^{-1}B \quad (4)$$

However, when the port number is very close to the number of nodes, it can only match the first one or two block moments of the original system, and cannot guarantee high accuracy. We present the theorems to further illustrate it. Below we assume the inputs J_e are impulses.

Theorem 1. *For single-input-single-output (SISO) system, when the q columns of projection matrix Q are obtained, the reduced transfer function* $\hat{h}(s) = \hat{l}(\hat{G} + s\hat{C} + \Gamma/s)^{-1}\hat{b}$ *matches the first q moments of the original transfer function* $h(s) = l(G + sC + \Gamma/s)^{-1}b$, *where* $b \in R^{N\times 1}$ [9].

Theorem 2. *For multiple-input-multiple-output (MIMO) system, when the q columns of projection matrix Q are obtained, the reduced transfer function* $\hat{H}(s) = \hat{L}(\hat{G} + s\hat{C} + \hat{\Gamma}/s)^{-1}\hat{B}$ *matches the first* $\lfloor q/p \rfloor$ *block moments of the original transfer function* $H(s) = L(G + sC + \Gamma/s)^{-1}B$, *where* $B \in R^{N\times p}$ [10].

See [6, 9, 10] for proofs of Theorem 1 and Theorem 2. Clearly, when there exits large number of ports, the matched block moment number will decrease. By introducing an excitation current source vector $J_{ex} = BJ_e$ to replace the incident matrix B, the original MIMO system is transformed into a superposed SISO system, in which RHS inputs are directly considered during reduction. This method is based on following Theorem.

Theorem 3. *Assume multiple-input-multiple-output (MIMO) system, and define the excitation current vector* $J_{ex} = BJ_e$

where $J_e \in R^{p\times 1}$ and $J_{ex} \in R^N$. When the q columns of projection matrix Q are obtained, the reduced nodal voltage variable $\hat{V}(s) = (\hat{G} + s\hat{C} + \hat{\Gamma}/s)^{-1}\hat{J}_{ex}$ matches the first q moments of the original $V(s) = (G + sC + \Gamma/s)^{-1}J_{ex}$.

PROOF. We note that the following two systems have the same output $V(s)$

$$\begin{aligned}(Gs + sC + \Gamma/s)V(s) &= BJ_e\\ (Gs + sC + \Gamma/s)V(s) &= J_{ex}.\end{aligned} \tag{5}$$

Note that J_{ex} can be decomposed into several excitation components J_i, where each J_i corresponds to the $i-th$ element of the J_{ex} vector.

$$J_{ex} = \sum_{i=1}^{p} J_i = \begin{bmatrix} J_1 \\ 0 \\ \vdots \\ \vdots \\ 0 \end{bmatrix} + ... + \begin{bmatrix} 0 \\ \vdots \\ J_p \\ \vdots \\ 0 \end{bmatrix} \tag{6}$$

Clearly for each J_i, it is equivalent to an SISO system with $b = J_i$. Therefore, $\hat{V}_i(s)$ matches the first q moments of $V_i(s)$. With superposition, it is easy to check that $\sum_{i=1}^{p}\hat{V}_i(s)$ matches the first q moments of $\sum_{i=1}^{p} V_i(s)$. □

Theorem 3 is also verified by experiments in Section 4. This theorem inspires us to develop a model order reduction approach, namely SAMSON, to directly match the moment of output voltage response considering multiple RHS sources.

2.2 Numerical Error of EKS/IEKS

Both EKS and IEKS use the incremental orthonormalization algorithm to find the projection basis. This algorithm, however, is numerically unstable and inaccurate. Mathematically, it is because the ith vector r_i depends on all the vectors from $1st$ to $(i-1)$th. [1]

The following vector r_i for the orthonormal basis is generated in [12]:

$$r_i = G^{-1}(\prod_{j=0}^{i-1}\alpha_j\mathcal{B}\bar{u}_i - \mathcal{C}(\widehat{r}_1 + \alpha_{i-1}\sum_{j=0}^{i-1}h_{i-1,j}\widehat{r}_j)) \tag{7}$$

For the simplicity of presentation, we denote $\mathcal{R} = \mathcal{G}^{-1}\mathcal{C}$ and assume that the directions of the orthonormalized basis, $\widehat{r}_i$, is not significantly influenced by the calculation error. But their norms are not strictly equal to 1. This assumption is reasonable because the entries in $\bar{r}_i$ are very close to zero and calculating their norms is error-prone in real cases. If minor error happens when we calculate $\alpha_0 = \frac{1}{||\mathcal{R}\bar{u}_0||}$ and we get $\tilde{\alpha}_{0e} = \alpha_0 + \delta\alpha_0$, then from (7), we have $r_{1e} = r_1 + \mathcal{R}\bar{u}_1\delta\alpha_0$ According to our assumption, the orthogonalized vector $\bar{r}_1$ has the same error bound as r_1 because the orthogonal process is in fact projecting r_1 along the direction represented by $\widehat{r}_0$. The result is not related to the norm of $\widehat{r}_0$. Therefore,

$$\begin{aligned}\tilde{\alpha_1} &= \frac{1}{||\bar{r}_{1e}||} = \frac{1}{||\bar{r_1} + \mathcal{R}\bar{u}_1\delta\alpha_0||}\\ &\geq \frac{1}{||\bar{r}_1|| + ||\mathcal{R}\bar{u}_1\delta\alpha_0||}\\ &= \frac{1}{||\bar{r_1}||}\frac{1}{1 + \frac{||\mathcal{R}\bar{u}_1\delta\alpha_0||}{||\bar{r_1}||}}\\ &= \frac{1}{||\bar{r_1}||}(1 - \frac{||\mathcal{R}\bar{u}_1\delta\alpha_0||}{||\bar{r_1}||} + \cdots)\end{aligned} \tag{8}$$

Using a first order approximation, we get $\tilde{\alpha_1} = \alpha_1 + \delta\alpha_1$, where $\delta\alpha_1 = \frac{||\mathcal{R}||}{||r_1||^2}\bar{u}_1\delta\alpha_0$. In general, we can get the similar recursive relationship between $\delta\alpha_i$ and $\delta\alpha_{i-1}, \delta\alpha_{i-2}, \cdots, \delta\alpha_0$ from (7), which shows how the error is propagated and amplified during the course of recursion:

$$\delta\alpha_i = \frac{||\mathcal{R}||}{||r_i||^2}\bar{u}_i\sum_{k=0}^{i-1}\delta\alpha_k \tag{9}$$

3. SAMSON METHOD

In this section, we present our SAMSON method considering multiple non-impulse sources of an RCS circuit. First, a generalized excitation current vector is introduced to transform the MIMO system into an equivalent superposed SIMO system with non-impulse sources. Then the augmented system transformation is employed to enable a linearization procedure. Therefore, the high order equation can be linearized into a set of linear equations. Finally, a projection matrix is found by a generalized second order Arnoldi method based orthonormalization for the resulted set of linear equations.

3.1 Generalized Excitation Current Vector

As we have mentioned in Theorem 3, excitation current vector can be used to transform an MIMO circuit into an equivalent superposed SISO one. As a result, q moments of the output can be matched instead of $\lfloor\frac{q}{p}\rfloor$ block moments from a projection matrix of order q.

Recall the definition of excitation current vector provided in Theorem 3. The *generalized excitation current vector* J_{ex} is the product of $\mathbf{B}$ and J_e, i.e., $J_{ex} = BJ_e(\in L^N)$. Each entry $\bar{J}_{ex}(s)$ in vector J_{ex} indicates the Laplace Transformation of the current source at one port.

We divide those current sources into two categories: rational (denoted as R-source) and irrational (denoted as I-source) according to their Laplace Transformations. Typical R-sources that are common in physical design include (attenuated) trigonometric sources like $sin(\omega t)$, $e^{-\alpha t}sin(\omega t)$, etc. Their Laplace transformations can be expressed as rational function of s:

$$\bar{J}_{ex}(s) = \frac{\bar{a}_0 + \bar{a}_1 s + \cdots + \bar{a}_n s^n}{\bar{b}_0 + \bar{b}_1 s + \cdots + \bar{b}_n s^m} \tag{10}$$

Typical I-sources that are common in physical design include impulses, PWL sources, and etc. The Laplace transformations of those sources cannot be expressed in rational form like R-sources.

To deal with the I-sources, we first expand them into series and take the dominant n+1 terms (from s^{-m} to s^{n-m}) as

[1] In the new orthogonalization procedure to be presented, r_i only depends on r_{i-1} and therefore is more accurate.

an approximation.

$$\bar{J}_{ex}(s) = \sum_{i=0}^{n} \bar{J}_i s^{i-m} \tag{11}$$

Experiments show that $n = 3$ can provide a maximum error less than 10^{-4}. $\bar{J}_{ex}(s)$ now can be viewed as (10) with $b_0, b_1, \cdots, b_{n-1}$ all equal to zero. From now on we will only discuss how to deal with R-sources in the form of (10).

Using (10), J(s) can be written as:

$$J_{ex}(s) = \frac{1}{b_0 + b_1 s + \cdots + b_n s^m} \begin{pmatrix} \sum_{i=0}^{n_1} a_i^1 s^i \\ \vdots \\ \sum_{i=0}^{n_p} a_i^p s^i \end{pmatrix} \tag{12}$$

Because in most applications we are interested in nodal voltage responses, we can obtain the following system equation in nodal analysis (NA) form with excitation current vector.

$$(sC + G + \frac{1}{s}\Gamma)V(s) = J_{ex}(s)$$

where $V(s)(\in L^N)$ is the nodal voltage vector, and G, C $(\in R^{N\times N})$ and $\Gamma = E_s S E_s^T$ are state matrices;

3.2 Augmented System Transformation

As we can see, the obtained J_{ex} can contain high order s terms both in nominator and denominator. However, in order to linearize the system, which will be discussed shortly after, we require the system to be in such an augmented form that the s^i term in LHS should have a correspondence in s^{i-1} term in RHS. This means that the highest order of s term in the LHS should be one order higher than that in the RHS.

Inserting (12) into (13) gives

$$\sum_{i=0}^{m+1} \Upsilon_i s^i V(s) = \sum_{i=0}^{n} \Theta_i s^i \tag{13}$$

where Υ_i and Θ_i can be directly calculated by expanding the polynomial product:

$$\Upsilon_i = Cb_{i-1} + Gb_i + \Gamma b_{i+1}, \Theta_i = [a_i^1, a_i^2, \cdots, a_i^p]^T. \tag{14}$$

We assume that in (13)the highest order of s in LHS is smaller than that of RHS, and remove this assumption later on. We first introduce a set of auxiliary variables V_i $(i = 1, 2, \cdots, n-m)$ to raise the order of LHS in (13)

$$V = sV_1, \quad V_1 = sV_2, \quad \cdots, V_{n-m-1} = sV_{n-m} \tag{15}$$

Set $U = [V, \quad V_1, \quad V_2, \quad \cdots, \quad V_{n-m}]^T$ as a new state vector, and we can transform the system equation into the following *augmented format*:

$$TU = \begin{bmatrix} \sum_{i=0}^{n} \Theta_i s^i \\ 0 \end{bmatrix} \tag{16}$$

where

$$T = \begin{bmatrix} 0 & 0 & 0 & 0 & \cdots & \sum_{i=0}^{m+1} \Upsilon_i s^{i+n-m} \\ I & -sI & 0 & 0 & \cdots & 0 \\ 0 & I & -sI & 0 & \cdots & 0 \\ & & & & & \\ 0 & 0 & \ddots & \ddots & \ddots & \vdots \\ 0 & 0 & 0 & I & -sI & 0 \end{bmatrix} \tag{17}$$

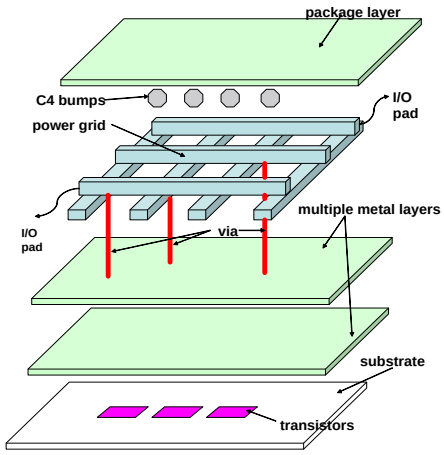

Figure 1: Diagram for package and power grid co-simulation.

$\in L^{N(n-m+1)\times N(n-m+1)}$. The new system is equivalent to the original one, except that the dimension is increased.

T can be further decomposed according to the descending order of s:

$$T = \Psi_{n+1} s^{n+1} + \Psi_n s^n + \cdots + \Psi_1 s + \Psi_0 \tag{18}$$

where

$$\Psi_i = \begin{cases} \begin{bmatrix} \mathbf{0} & \Upsilon_i \\ \mathbf{0} & \mathbf{0} \end{bmatrix}, & i \geq 2 \\ \begin{bmatrix} \mathbf{0} & \Upsilon_1 \\ \mathbf{0} & \mathbf{0} \end{bmatrix} + \begin{bmatrix} \mathbf{0} & \mathbf{0} \\ \mathbf{0} & -I \end{bmatrix}, & i = 1 \\ \begin{bmatrix} \mathbf{0} & \Upsilon_0 \\ \mathbf{0} & \mathbf{0} \end{bmatrix} + \begin{bmatrix} \mathbf{0} & \mathbf{0} \\ I & \mathbf{0} \end{bmatrix}, & i = 0 \end{cases} \tag{19}$$

Inserting (18) into the new system equation (16), the system equation can be rewritten in the descending order of s term:

$$\sum_{i=0}^{n+1} \Psi_i s^i U = \begin{bmatrix} \sum_{i=0}^{n} \Theta_i s^i \\ 0 \end{bmatrix} \tag{20}$$

Note that if the LHS in (13) has a higher order than RHS, then it is not necessary to raise the order of LHS and (20) can be directly obtained.

3.3 System Linearization

As we can see, (20) is a high order equation and cannot be directly used to find the projection matrix. Therefore, we introduce a set of auxiliary variables to linearize it into a set of linear equations.

Shifting (20) with $s = s_0 + \sigma$, we have

$$\sum_{i=0}^{n+1} A_i \sigma^i U(\sigma) = \sum_{i=0}^{n} R_i \sigma^i \tag{21}$$

where $A_i = \sum_{k=i}^{n+1} C_k^i \Psi_i s_0^{k-i}$ and $R_i = \begin{bmatrix} \sum_{k=i}^{n} C_k^i s_0^{k-i} \Theta_i \\ 0 \end{bmatrix}$. These coefficient matrices can be directly derived from polynomial expansion in (20).

Again introducing a set of new variables $Z_i(\sigma)(i = 1, \cdots, n)$ satisfying

$$\begin{aligned} A_{n+1}U + \sigma Z_n &= R_n \\ \sigma(A_n U - Z_n) + Z_{n-1} &= R_{n-1} \\ \sigma(A_{n-1}U - Z_{n-1}) + Z_{n-2} &= R_{n-2} \\ &\cdots \\ \sigma(A_2 U - Z_2) + Z_1 &= R_1, \end{aligned} \tag{22}$$

and substituting (22) into (21), we have

$$(A_0 + A_1\sigma)U - \sigma Z_1 = R_0 \tag{23}$$

Combing (23) and (22) and noticing that the first N rows of U is exactly the original state variable V in (13), we get

$$(I - \sigma A)\begin{bmatrix} V \\ D \end{bmatrix} = \begin{bmatrix} q_0 \\ p_0 \end{bmatrix} \tag{24}$$

where

$$A = \begin{bmatrix} -A_0^{-1}A_1 & 0 & \cdots & A_0^{-1} \\ -A_{n-1} & 0 & \cdots & 0 \\ -A_{n-2} & 0 & \cdots & 0 \\ \vdots & \vdots & \ddots & \vdots \\ -A_2 & 0 & \cdots & I \end{bmatrix} \tag{25}$$

and

$$D = \begin{bmatrix} U(N+1:(n-m)N) \\ Z_n \\ \vdots \\ Z_1 \end{bmatrix} \tag{26}$$

If we denote $M = \begin{bmatrix} A_0^{-1}R_0 & R_n & R_{n-1} & \cdots & R_1 \end{bmatrix}^T$, then $q_0 = M(1:N)$ and $p_0 = M(N+1:(n+1)(n-m)N)$.

By moving $(I - \sigma A)$ to the RHS of (24) and performing a Maclaurin series expansion, we have

$$\begin{bmatrix} V \\ D \end{bmatrix} = (I + \sigma A + \sigma^2 A^2 + \cdots)\begin{bmatrix} q_0 \\ p_0 \end{bmatrix} \tag{27}$$

Obviously, $A^{i-1}\begin{bmatrix} q_0 \\ p_0 \end{bmatrix}$ is the i-th moment of $\begin{bmatrix} V \\ D \end{bmatrix}$, q_0 and p_0 are actually the first moments of V and R, respectively.

Equation (24) is a linearized form of (21) with RHS independent of σ. If $\begin{bmatrix} V \\ D \end{bmatrix}$ is the solution to (24), then V must be the solution to (13). Therefore, the upper part of the i-th moment $\begin{bmatrix} V \\ D \end{bmatrix}$, i.e. $\begin{bmatrix} I & \mathbf{0} \end{bmatrix} A^{i-1}\begin{bmatrix} q_0 \\ p_0 \end{bmatrix}$, should be equal to the i-th moment of the output V. In addition, note that although the dimension of (24) is augmented due to introduced high-order auxiliary state variables, (24) can be efficiently factorized in a recursive fashion because of the lower triangular structure of A matrix.

3.4 Projection

In order to construct an orthonormal basis q_i for the projection matrix Q, we employ a similar procedure as the SOAR algorithm presented in [14]. However, there is one important difference that distinguishes our projection method with theirs. As we have discussed above, we deal with B and J matrices together as J_{ex}, so we should also project on J_{ex}. Once we obtain Q, we perform an orthogonal projection on the original second-order system (13), and get the

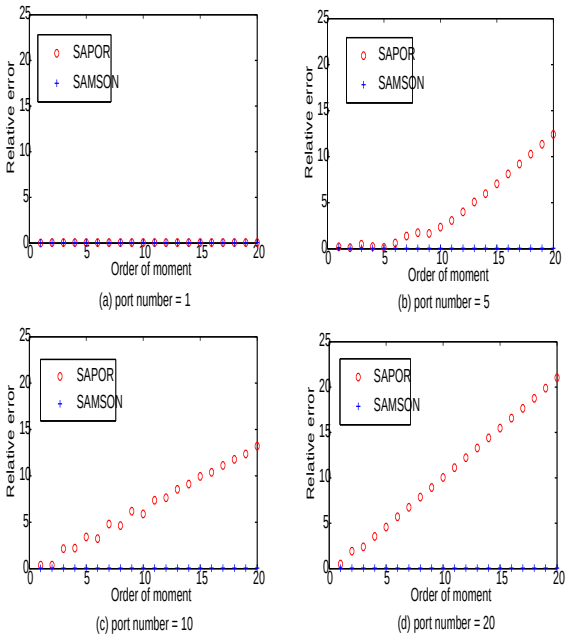

Figure 2: Relative error of Moment matching for an RCS mesh with regard to port number.

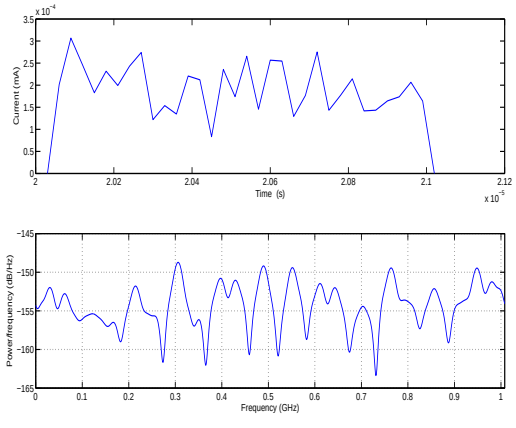

Figure 3: Waveform and spectrum of a typical PWL current source modeled from FPGA circuits.

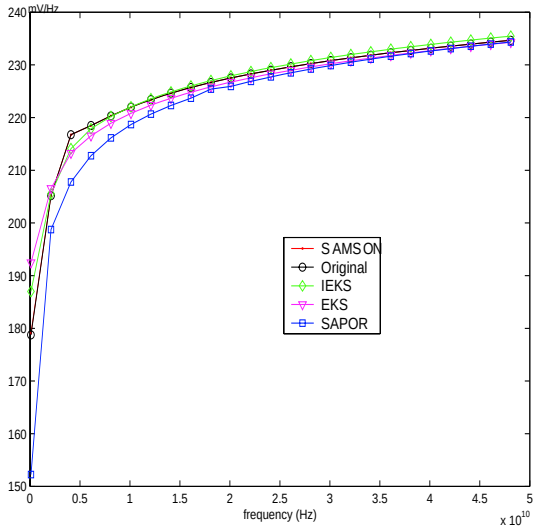

Figure 4: Frequency domain response comparison between SAMSON, IEKS, EKS, SAPOR and original with PWL sources. SAMSON is identical to the original.

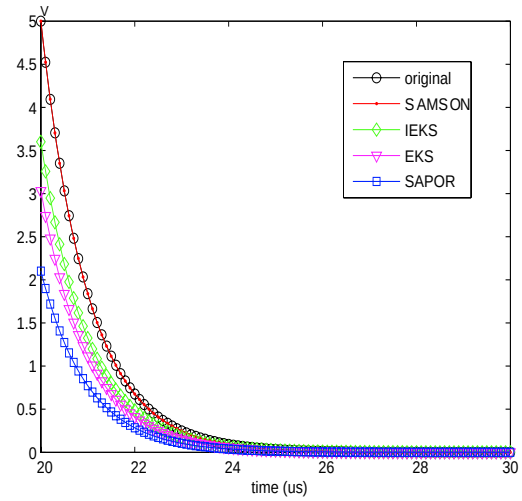

Figure 5: Time domain response comparison between SAMSON, IEKS, EKS, SAPOR and the original with PWL sources. SAMSON is identical to the original.

reduced-order system in the same form.

$$(s\widehat{C} + \widehat{G} + \frac{1}{s}\widehat{\Gamma})\widehat{V}(s) = \widehat{J}_{ex}(s) \tag{28}$$

where $\widehat{C} = Q^T CQ$, $\widehat{G} = Q^T GQ$, $\widehat{\Gamma} = Q^T \Gamma Q$, $\widehat{V} = Q^T V$ and $\widehat{J}_{ex} = Q^T J_{ex}$

Since C, G, Γ are all symmetry positive semi-definite, it is proved in [7] that the orthogonal projection preserves the passivity of the original system. We can conclude that the reduced-order system in (28) has guaranteed passivity, too.

Based on Theorem 3, we can see that SAMSON can match the first q moments of the output V if the projection matrix Q has q columns. The essence of SAMSON is to convert a MIMO circuit into a superposed SIMO one with equivalent output. This is exactly the reason why SAMSON can outperform the non-RHS MOR methods like PRIMA and block-SAPOR [10] when there are multiple sources. When we reduce the circuit to order q, SAMSON can match the first q moments of the output vector. In contrast, non-RHS MOR methods can only match the first $\lfloor q/p \rfloor$ block moments of the transfer function and accordingly the first $\lfloor q/p \rfloor$ moments of the output vector after convolution.

The orthonormalization in SAMSON is numerically more stable than EKS [12]. First, in SAMSON the new projection vector is generated only by the orthonormalized previous one, thus avoiding the error amplification. In contrast, the projection vector by EKS needs all previous ones. As discussed in Section II, it introduces accumulated numerical error. Furthermore, techniques as described in [14] can be employed to deal with the deflation cases, which further improves the stability of the orthonormalization in SAMSON.

4. NUMERICAL EXPERIMENTS

In this section, we present the numerical experiments to demonstrate the efficiency and accuracy of the proposed SAMSON method and compare it with EKS, IEKS and block-SAPOR. Here we choose block-SAPOR as a representative of non-RHS MOR methods because it has higher accuracy compared with ENOR and SMOR for RCS circuits [9]. All methods are implemented in MATLAB, and run on PC with Intel Pentium IV 2.66G CPU and 1G RAM. We use the extracted RCS meshes to model power plane in package, RC meshes to model on-chip power/ground grids, and RC elements to model vias and bumps that connect off-chip package plane and on-chip power/ground grid. The examples to be presented are from real industrial applications. An illustration of package and power grid is shown in Figure 1. Moreover, we first perform model order reduction to obtain frequency domain response, then carry out IFFT (Inverse Fast Fourier Transformation) with 1024 sampling points to obtain the time-domain response.

4.1 Moment Matching

Theorem 2 and 3 are experimentally verified in Figure 2. We use an example of a package-grid model with 192 nodes and unit impulses are added at 1, 5 , 10 and 20 ports respectively. Both block-SAPOR and SAMSON use order $q = 20$ for the reductions. Clearly shown in Figure 2, block-SAPOR can only match $\lfloor q/p \rfloor$, i.e., 20, 4, 2 and 1 moments respectively. On the other hand, SAMSON can constantly match 20 moments, independent of the port number.

4.2 RHS Non-impulse Source Reduction

We first consider the above package model with 50 ports excited by PWL sources. We reduce the circuit to order q=80, and measure the output by randomly selecting the output ports. The PWL current sources are generated from HSPICE characterization of FPGA circuits. Its magnitude are different at different ports. An example of such waveform and its spectrum (analyzed by Welch method from MATLAB) are shown in Figure 3 (a) and (b).

The frequency domain response is shown in Figure 4. Clearly, we can see that SAMSON matches exactly with the original model. On the other hand, IEKS shows small

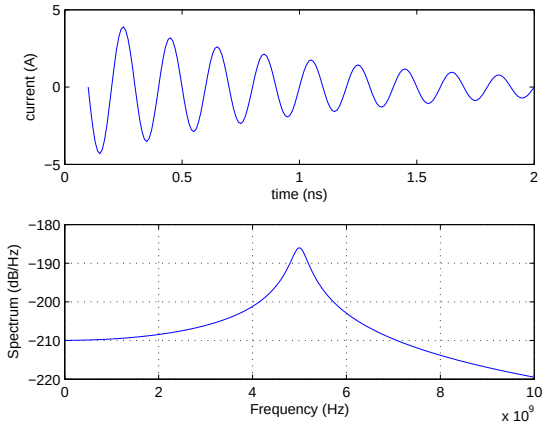

Figure 6: Waveform and spectrum of a typical attenuated sine current source.

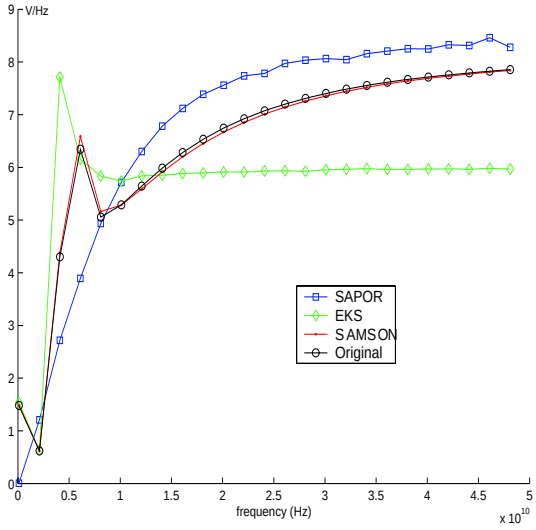

Figure 7: Frequency domain response comparison between SAMSON, EKS, SAPOR and the original with attenuated sine sources.

error at lower frequencies. Although worse than IEKS at both low frequency and high frequency ranges, EKS outperforms block-SAPOR significantly. This is because SAPOR can only match the first block moment of the original system in this case. It further illustrates the advantage of RHS MOR methods.

We also compare the time domain simulation in Figure 5. In finite time period, the input PWL sources vanish and the output voltage falls to zero. It is clear that the reduced model by SAMSON exactly matches the original waveform, which approaches zero much faster than the waveforms for the other models. This is because as shown in Figure 4, the output of SAMSON produces the largest high frequency content than the other methods.

Finally, we use the same circuit above for SAMSON, EKS and block-SAPOR, but apply attenuated sine waveforms in Figure 6. The frequency domain and time domain results are compared in Figure 7 and Figure 8, respectively. We

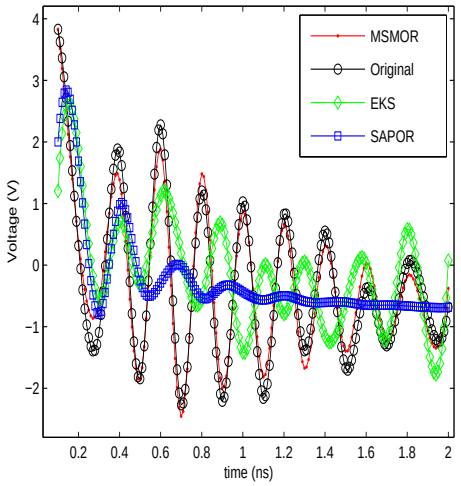

Figure 8: Time domain response comparison between SAMSON, EKS, SAPOR and original with attenuated sine sources.

did not take IESK into consideration because it cannot handle sources with $1/s^i$ $(i > 0)$ terms. From Figure 7 we can see that SAMSON still matches the original output exactly. EKS, however, can only match well at *dc* and low frequency range, and it has large error in the high frequency range. This is mainly because EKS can only expand and take the first several moments of the input sources as an approximation to match the original system. It neglects the higher order terms that are important to match high frequency behavior.

4.3 Scalability Study

Figure 9 shows the average time domain waveform error of SAMSON, IEKS, EKS and SAPOR compared to the original result with respect to the reduction order. We perform reductions on several different sized package-grid circuits with around 200-70000 nodes. For each circuit 30% nodes have PWL sources. It is clear that with the increase of order, SAMSON approaches to the accurate solution faster than IEKS/EKS and block-SAPOR, where the error of block-SAPOR is not reduced consistently. At order 40, SAMSON reduces error by 47X compared with block-SAPOR and by 33X compared with EKS/IEKS methods.

The runtime complexity comparison for above circuits in Figure 9 is studied in Table 2. Compared with EKS/IEKS, SAMSON has smaller reduction time due to its higher accuracy, but the time growth has a similar trend. For a RLC mesh with 11520 nodes and 800 ports, it is 25X faster than the direct simulation without reduction.

5. CONCLUSIONS AND DISCUSSIONS

In this paper, we have presented a generalized Second-order Arnoldi method for reducing Multiple SOurce Network, namely SAMSON. It can handle linear RCS circuits with large numbers of non-impulse current sources. We replace the port incident matrix by a generalized right-hand-side excitation current vector such that an MIMO system is transformed into an equivalent superposed SIMO system.

# of nodes	# of sources	Cir Sim Time (s)	Reduction + Simulation Time (s)		
			EKS	IEKS	SAMSON
192	50	0.18	0.11+0.00	0.09+0.00	0.08+0.00
768	100	106	10.4+0.4	10.2+0.4	7.6+0.4
2048	200	362	20.6+0.8	20.4+0.8	15.8+0.8
11520	800	1164	66.1+3.2	65.2+3.2	47.3+3.2
69380	4000	N/A	384+92	381+92	295+92

Table 2: Comparison of the reduction and simulation time under the same accuracy up to 50GHz.

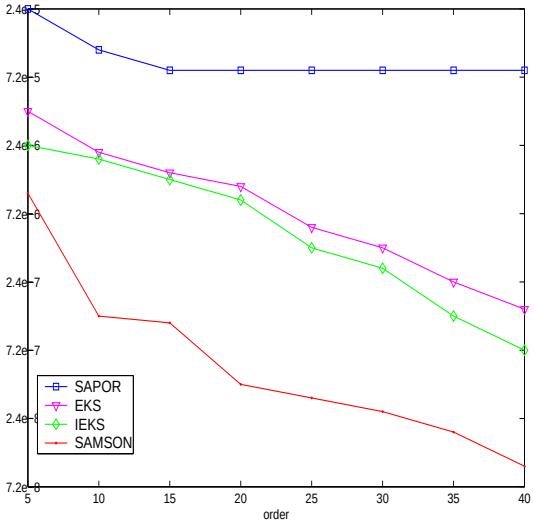

Figure 9: Error comparison between SAPOR, IEKS, EKS and SAMSON with respect to order.

This avoids accuracy loss in block moment matching. In addition, the system equation with susceptance and generalized right-hand-side excitation current vector, can be linearized into an augmented system by introducing auxiliary state variables. The augmented system can be reduced by a generalized second-order Arnoldi method. with improved accuracy during orthonormalization. Compared with existing EKS and IEKS approaches, SAMSON is able to consider both non-impulse sources and susceptance. Moreover, SAMSON is more accurate in both high frequency range and at *dc*. With the use of same model order, SAMSON reduces time domain waveform error by 33X compared to EKS/IEKS and by 47X compared with SAPOR, the best block moment matching method applicable to susceptance.

6. REFERENCES

[1] D. Ling and A. Ruehli, *Circuit Analysis, Simulation and Design - Advances in CAD for VLSI*, vol. 3. Elsevier Science Publisher, 1987.

[2] A. Devgan, H. Ji, and W. Dai, "How to efficiently capture on-chip inductance effects: introducing a new circuit element K," in *Proc. Int. Conf. on Computer Aided Design (ICCAD)*, pp. 150–155, 2000.

[3] M. Beattie and L. Pileggi, "Efficient inductance extraction via windowing," in *Proc. European Design and Test Conf. (DATE)*, pp. 430–436, 2001.

[4] M. Zhao, R. V. Panda, S. S. Sapatnekar, and D. Blaauw, "Hierarchical analysis of power distribution networks," *IEEE Trans. on Computer-Aided Design of Integrated Circuits and Systems*, no. 2, pp. 159–168, 2002.

[5] E. Chiprout, "Fast flip-chip power grid analysis via locality and grid shells," in *Proc. Int. Conf. on Computer Aided Design (ICCAD)*, 2004.

[6] A. Odabasioglu, M. Celik, and L. Pileggi, "PRIMA: Passive reduced-order interconnect macromodeling algorithm," *IEEE Trans. on Computer-Aided Design of Integrated Circuits and Systems*, pp. 645–654, 1998.

[7] B. N. Sheehan, "ENOR: Model order reduction of RLC circuits using nodal equations for efficient factorization," in *Proc. Design Automation Conf. (DAC)*, 1999.

[8] H. Zheng and L. T. Pileggi, "Robust and passive moel order reduction for circuits containing susceptance elements," in *Proc. Int. Conf. on Computer Aided Design (ICCAD)*, 2002.

[9] Y. Su, J. Wang, X. Zeng, Z. Bai, C. Chiang, and D. Zhou, "SAPOR: Second-Order Arnoldi Method for Passive Order Reduction of RCS Circuits," in *Proc. Int. Conf. on Computer Aided Design (ICCAD)*, 2004.

[10] B. Liu, X. Zeng, Y. Su, J. Tao, Z. Bai, C. Chiang, and D. Zhou, "Block SAPOR: Block Second-Order Arnoldi Method for Passive Order Reduction of Multi-Input Multi-Output RCS Interconnect Circuits," in *Proc. Asia South Pacific Design Automation Conf. (ASPDAC)*, 2005.

[11] E. Chiprout and T. Nguyen, "Power Analysis of large interconnect grids with multiple sources using model reduction," in *European Conference on Circuit Theory and Design*, 1999.

[12] J. M. Wang and T. V. Nguyen, "Extended Krylov Subspace Method for Reduced Order Analysis of Linear Circuits with Multiple Sources," in *Proc. Design Automation Conf. (DAC)*, 2000.

[13] Y. Lee, Y. Cao, T. Chen, J. Wang, and C. Chen, "HiPRIME: Hierarchical and Passivity Preserved Interconnect Macromodeling Engine for RLKC Power Delivery," *IEEE Trans. on Computer-Aided Design of Integrated Circuits and Systems*, vol. 26, no. 6, pp. 797–806, 2005.

[14] Z. Bai and Y. Su, "SOAR: A Second-Order Arnoldi Method for the Solution of the Quadratic Eigenvalue Problem," *SIAM J. Matrix Anal. Appl.*, vol. 26, no. 3, pp. 640–659, 2005.